Analyzing the Electromagnetic Radiations Emitted during a Laser-based Surface Pre-Treatment Process for Aluminium using Diode Sensors as an Approach for High-Resolution Online Monitoring

Hans Julius Langeheinecke[*1,2], Shahan Tutunjian[1], Marcos Soldera[2], Torsten Wegner[1], and Andrés Fabián Lasagni[2,3]

[1]*Verbindungstechnik Schweißverfahren, Schrauben, BMW AG, 80788 Munich, Germany*
[2]*Institut für Fertigungstechnik, Technische Universität Dresden, 01069 Dresden, Germany*
[3]*Fraunhofer–Institut für Werkstoff und Strahltechnik (IWS), Winterbergstr. 28, 01277 Dresden, Germany*
[*]*Corresponding author's e-mail: hans-julius.langeheinecke@bmw.de*

To obtain a good adhesive bonding quality between aluminum parts it is necessary to remove contaminations and to define the chemical composition and topographic status of the corresponding surfaces. Hence, a surface pre-treatment is needed which simultaneously guarantees environmental concerns, industrial safety, efficiency, and reproducibility of surface quality. For this purpose, nano-second-pulsed laser processing is suitable, especially concerning the integration of the surface pre-treatment process in the main processing line of the body shop. To fulfill the technical requirements and to minimize the production of scrap parts, an online monitoring and control system of the pre-treatment process is essential. In this study, electromagnetic radiations, which are generated by the laser-based pre-treatment process, are detected online using photodiodes. The recorded signals are examined in terms of the correlation between their dynamics, the resulting surface state (quality of the pre-treatment) and the executed process/system parameters. Conventional offline methods for analyzing the chemical composition and topography of surfaces are applied to validate the results. It was found that the obtained information can be used to define a process window and enable the development of a proper process monitoring and control system for the laser-based pre-treatment process for industrial use.

DOI: 10.2961/jlmn.2022.03.2002
Keywords: surface pre-treatment, ns-pulsed laser, aluminum, online monitoring, diode sensors

1. Introduction

Adhesive bonding of aluminum and their alloys is increasingly used in the automotive industry due to the potential for lighter cars, with the corresponding reduction of emissions and fuel consumption. Additionally, Al-alloys have further beneficial properties, such as high resistance against corrosion, formability, and recycling potential [1-3].

To obtain good adhesive bonding qualities, laser-based surface pre-treatment of the Al components is an effective, ecologically friendly, and industrially feasible method to prepare the corresponding surfaces [4-11]. Furthermore, it was demonstrated that the method generates clean surfaces with the required surface roughness and chemical composition [6, 12, 13]. Both efficiency and process stability play an important role in terms of cost-effective and industrial production [14]. Hence, process monitoring methods are necessary to ensure appropriate process stability and to reduce the production of scrap parts [15].

Various established monitoring approaches are suitable for laser manufacturing processes including laser welding and cutting, as well as laser-based additive manufacturing. These approaches are based on the detection of different physical signals, such as acoustic, optical, or thermal, by using specific sensors [16-19]. Although laser-based surface processing monitoring methods have not been extensively developed, in recent years several approaches have been reported. For instance, topographical features, like pattern geometry or structure depth, can successfully be monitored using scatterometry-based systems [20-25]. These monitoring approaches either need a separate light source or have been so far utilized offline, as a post-process characterization method. Other approaches use free-field or omnidirectional microphones, that can detect acoustic emissions and for instance correlate their signal intensity with material ablation allowing the determination of the focal position [26-29]. Furthermore, other approaches allow the precise determination of the ablation threshold regarding the needed power and the ablation rate of material, respectively, by using acoustic and optoacoustic imaging methods [30-32] Information on temperature distribution, which can be correlated with heat accumulation during laser processing, can be monitored using infrared thermography [33-35]. Other approaches use photodiodes or spectrometers for detecting electromagnetic emissions that can provide information on both the thermal distribution, the plasma torch formation, and the back reflection of laser beam radiation [23, 36-38].

However, none of these methods have been implemented with high-temporal resolution in an industrial environment. Hence, the objective of this work is the development of an online monitoring approach for laser-based surface pre-treatment of aluminum parts. This strategy uses photo-

diodes to analyze the electromagnetic radiation emitted during the process. Different laser parameters are varied including the laser power, laser repetition rate and geometrical irregularities of the sample material. The relationship between the detected emissions, the resulting quality of the surfaces, and the process parameters is investigated.

2. Experimental procedure

2.1 Materials

Sheets of aluminum (Al 5754) with lateral dimensions of 55 mm × 600 mm and a thickness of 2 mm were used in this study. The initial surface roughness S_a of the parts was 0.4 µm ± 0.02 µm (measured according to DIN ISO 25178 [39]). This alloy is relevant for structural adhesive bonding applications in both car body and high voltage battery production. The samples were gently cleaned from contamination (e.g. oil and dust particles induced by handling and storage) using isopropanol prior to the laser pre-treatment process.

2.2 Laser surface pre-treatment setup

The samples were processed with an industrial high-performance ns-pulsed laser beam source (TruMicro 7070, Trumpf, Germany) using a high dynamic performance scan system (IntelliSCAN 30, Scanlab, Germany) equipped with an f-theta lens with a focal distance of 420 mm (S4LFT0420/126, Sill Optics, Germany) allowing a working distance of approximately 570 mm. The laser system operated at a wavelength of 1030 nm with a variable repetition rate from 5 kHz to 250 kHz and a fixed pulse duration of 30 ns. The processing head was mounted to an industrial handling robot (KR 210 R3100 ultra, Kuka, Germany) for automatized positioning. The square-shaped laser spot with an edge length (dL) of 1800 µm was kept constant during all experiments. Process parameters such as laser power (P), pulse energy (E_p), repetition rate of the laser (f_L), pulse overlap (O_p), line overlap (O_l), and scanning velocity (v_s) were varied. Table 1 shows the different process parameters used for the pre-treatment procedure in this study including the initial geometrical conditions of the samples and geometrical irregularities investigated in this work. The geometrical irregularities were generated using overlapping sheets that were joined together with laser tack welds.

To study the influence of the power variation using the monitoring process, two series of experiments were conducted. Firstly, only the average laser power was varied whereas negative pulse and line overlaps were used and kept constant (see Table 1, Series 1). Furthermore, defined surface irregularities such as tack weld roots and the edge of flat overlapping sheets with an overlap of 25 mm were generated in a second experimental series (see Table 1, Series 2). The laser pre-treated area for the experiments in Series 1 was 40 mm × 100 mm while the area for the Series 2 was 40 mm × 90 mm.

Table 1 Process parameters used for the laser-based surface pre-treatment of the aluminum specimen (P: average laser power, E_p: pulse energy f_L: repetition rate, O_l: line overlap, O_p: pulse overlap; v_s: scanning speed) including geometrical settings of the samples.

Parameter	Series 1	Series 2
P [W]	197; 590; 983	1966
E_p [mJ]	19.7; 59.0; 98.3	98.3
f_l [kHz]	10	20
O_l [%]	-10	15
O_p [%]	-10	90
v_s [m/s]	19.8	21.0
geometrical setting	flat sheet	edge and tack weld roots of overlapping sheets

Fig. 1 shows schematically (a) the experimental setup and (b) the used scanning strategy throughout the experiments.

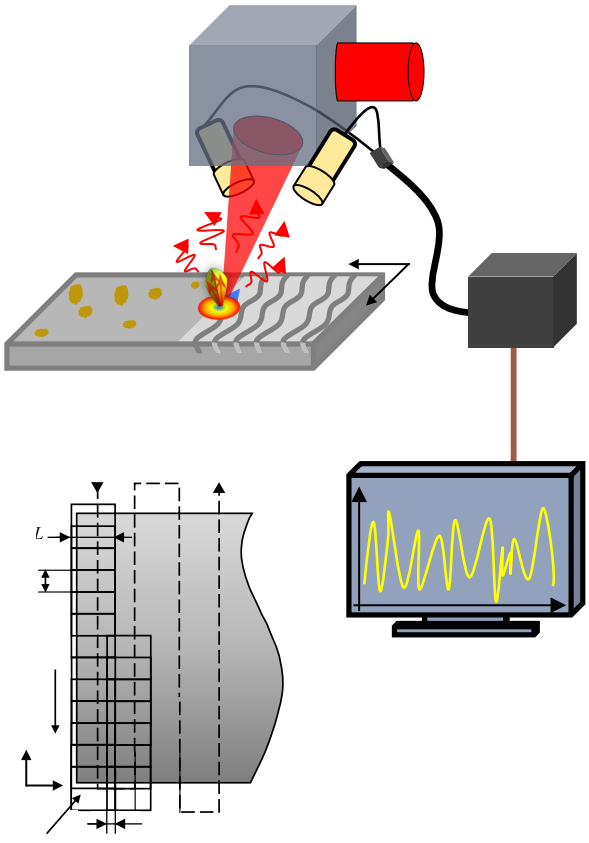

Fig. 1 (a) Laser surface pre-treatment and monitoring setup with (1) laser processing head, (2) laser source, (3) Al-specimen with (4) surface contaminations, (5) radiation collecting units including connector and optical fibers, (6) diode sensors in housing, (7) process monitoring and control unit including Human Machine Interface (HMI), and (b) schematics of used scanning strategy.

2.3 Monitoring setup

To detect the electromagnetic emissions during the pre-treatment process, a real-time photodiode-based monitoring system (Processobserver, Plasmo, Austria) was used, having a nominal spectral sensitivity between 400 nm to 1100 nm and a maximum sampling rate of 250 kHz. The radiation collecting units were attached to the laser processing head facing the sample under treatment. The specific position toward the processing zone has been optimized to detect the electromagnetic radiations with the highest signal-to-noise ratio intensity as possible. An illustration of the monitoring setup is shown in Fig. 1a.

The emissions were collected by two units and merged into a single optical fiber that leads to the sensor box. Then the radiations were detected by a photodiode with a filtered detectivity range of 750 nm to 1100 nm. This spectral range allows the observation of thermal phenomena on the surface, plasma formation, as well as reflection phenomena of laser radiation on the irradiated surface [40]. The spectral sensitivity was defined by using an optical filter (Cut on 750 nm, bk Interferenzoptik, Germany) permeable for the specific range of wavelengths. A sampling rate of 250 kHz, which is more than ten times higher than the pulse repetition rate used in the laser texturing experiments, and the optical filtering setup were kept constant during all experiments.

The diode sensor converts the detected electromagnetic emissions into an electrical signal response. The amplitude of these signals represents the intensity of the detected emissions, and it is displayed as dimensional counts. Finally, the recorded data were processed using common statistical algorithms for data analysis.

2.4 Surface characterization

The surface topography of the processed samples was characterized using confocal microscopy (CM) with a 20x magnification objective (S Neox, Sensofar, Spain). The vertical and optical resolutions of the used objective were 8 nm and 310 nm, respectively. The software SensoMap® 7.3 (Sensofar, Spain) was utilized to analyze the measured surface topography data. In addition, the chemical or elemental compositions of the initial and processed samples were characterized using X-ray photoelectron spectroscopy (XPS, PHI 5000 VersaProbe II, ULVAC-PHI, Japan) with a beam size of 100 µm and pass energy of 187.85 eV under ultra-high vacuum conditions. The amount of carbon residue on the surface is a measure of the cleaning efficiency of the laser pre-treatment.

3. Results and discussion

Surfaces of aluminum sheets were laser pre-treated varying the laser power P, the repetition rate f, and the pulse/line overlaps $O_{p/l}$. In addition to that, samples with geometrical irregularities, consisting of the edge and the tack weld roots of two overlapping flat sheets, were laser processed as well. The experiments were carried out five times for every set of parameters to ensure statistical reliability.

3.1 Analysis of topographic features

Exemplary CM images of the obtained structures at different laser power together with the initial surface are shown in Fig. 2a. Also, corresponding optical micrographs are depicted in Fig. 2b. These images permit a qualitative evaluation of the surface quality after the laser treatment.

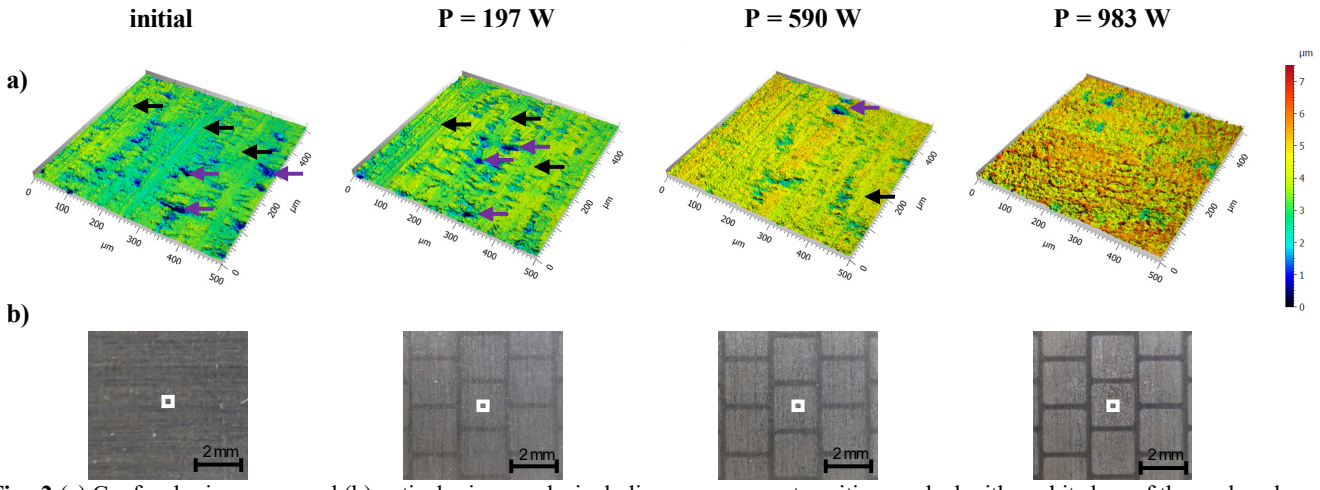

Fig. 2 (a) Confocal microscope and (b) optical micrographs including measurement position marked with a white box of the analyzed surfaces of the Series 1. Arrows in (a) exemplary indicate positions of crater-like depressions (purple) and grooves (black).

The topography of the initial sample surface, which was not processed with the laser, shows conspicuous features such as punctual depressions and grooves (see indicating arrows in Fig. 2a). The roughness S_a of this surface was 0.40 µm ± 0.02 µm (see Fig. 3a). The corresponding photographic image in Fig. 2b indicates homogenous, horizontally arranged lines, which have been caused by the manufacturing process of the sample material.

Samples processed with a laser power of 197 W show very similar topographic features as in the initial samples. Some of the punctual depressions tended to vanish compared to the reference surfaces and a slight decrease in grooves depths is visible. In this case, the Al-samples had a surface roughness S_a of 0.46 µm ± 0.07 µm. The corresponding optical micrograph shows the typical markings (squares) on the surface generated by the laser pulses.

Using a laser power of 590 W, the resulting surface topography showed a general increase in features depth and a reduced occurrence of grooves and punctual depressions. Also, in this case, the surface roughness was similar to the previous cases (S_a = 0.47 µm ± 0.07 µm). From the optical micrographs (Fig. 2b), the produced square areas are more noticeable through sharply shaped spot markings on the surface.

As expected, the highest laser power of 983 W had the largest impact on the surface topography. There were neither grooves nor any crater-like depressions on the resulting surface. This can be explained by the stronger melting process induced by the laser radiation. In this case, the surface roughness was significantly higher, with a value S_a of 0.53 µm ± 0.06 µm. From the CM image, it is also visible that the topography shows multiple rounded bulges, which can be explained by the melting of the Al-surface.

Finally, the effect of the laser power on the surface roughness as a function of the average laser power is indicated in Fig. 3a. As mentioned before, the surface roughness increased with the laser power. Other roughness parameters have been used for a better evaluation of the laser treatment on the morphological characteristics of the Al-surfaces. Namely, the skewness S_{sk} and kurtosis S_{ku} parameters are suitable to characterize surfaces with similar S_a values, but with different shapes [41]. In particular, the skewness parameter describes the symmetry of the height distribution about the mean line. Its value depends on whether most of the material is located above (negative skewed) or below (positive skewed) the mean line. On the other hand, the kurtosis parameter is related to the sharpness of the surface height distribution, and it is very sensitive to occasional high peaks or deep valleys [41, 42]. The kurtosis (S_{ku}) and skewness (S_{sk}) for the treated surfaces as function of the laser power for the experiments in Series 1 including the reference sample are illustrated in Fig. 3b and 3c, respectively.

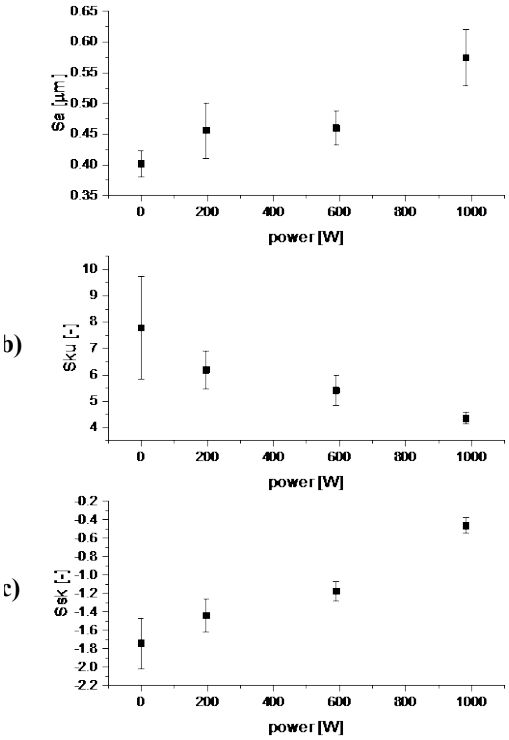

Fig. 3 (a) Arithmetic mean roughness S_a, (b) Kurtosis S_{ku}, and (c) Skewness S_{sk} of analyzed samples within the Series 1 as a function of employed laser power. Whereas P = 0 W represents results for the untreated reference samples.

The initial samples had the highest kurtosis and the lowest skewness of all analyzed samples. Taking into account the 3D CM plots, these values can be explained by the many sharp valleys or peaks as well as due to the fact that the observed punctual depressions are very deep, and most of the material is located below the mean height of the surface [43].

As the laser power increases, a decrease in kurtosis and an increase in skewness were observed. In the case of S_{ku}, a reduction from 7.79 (untreated material) to 4.35 (at 983 W) is observed. This trend points at a significant change in the surface morphology, from a dominant distribution of sharp valleys and peaks to a smoother surface. In other words, the heights histogram of the surface tended to be more likely to have a Gaussian distribution (S_{ku} = 3) as the power increased. Differently, S_{sk} increases from -1.74 to -0.46. These results can be explained from one side by the melting of the surface, reducing the depth of the initial grooves and their rounded geometry. Furthermore, the topography tended to be distributed more symmetric to the mean line (S_{sk} = 0) with increasing power.

3.2 Analysis of surface chemical composition

For evaluating the cleaning efficiency of the laser treatment, XPS analyses were performed. The presence of chemical species such as carbon (C 1s) is an indicator of the cleaning efficiency. The results of XPS analysis are illustrated in Fig. 4.

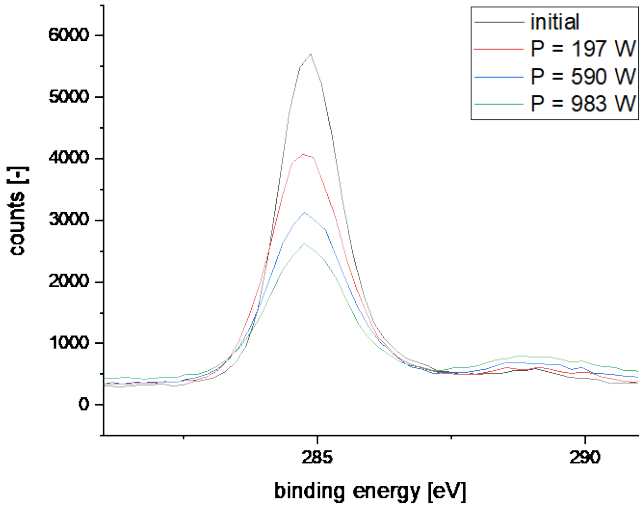

Fig. 4 XPS high-resolution spectra of C 1s of laser pre-treated samples with varying power together with the reference surface.

The XPS spectra presented peaks at a binding energy of 285 eV, which is attributed to C 1s [44]. It is observed an inverse relationship between the used laser power and signal intensity for the mentioned peak. This trend indicates an increasing cleaning efficiency of carbon residues on the surface with increasing laser power.

3.3 Analysis of electromagnetic radiations

In addition to the topographical and chemical analysis of the samples, the electromagnetic emissions obtained during the laser-based pre-treatment process were evaluated to study the impact of the laser energy on the corresponding surface. Photodiode-based sensors were used to detect the electromagnetic radiations and to convert these into an electrical signal response that can be digitalized and analyzed.

Due to the high robustness of the process, a single signal was recorded and analyzed in this study and considered representative of the process. An exemplary photograph of the resulting surface after the laser treatment using a laser power of 983 W is illustrated in Fig. 5a. The square-shaped lighter areas in Fig. 5a represent the laser-modified surface, each of which was irradiated with a single pulse. According to the scanning strategy presented in Fig. 1b, the pulses were scanned along a line in the y-direction, followed by a displacement in the x-direction and a successive scan in the y-direction following a meander-like path, until the complete area was structured. The scanning direction in negative or positive y-direction is marked with orange and blue arrows, respectively. The captured electromagnetic emissions generated during the processing of the sample using the diode-based monitoring system are exemplarily shown in Figs. 5b, c. Each single processed vertical line on the sample generated a global peak in the signal curve. Additionally, the results of the fast Fourier transformation (FFT) of the corresponding signals are exemplarily shown in Fig. 5e.

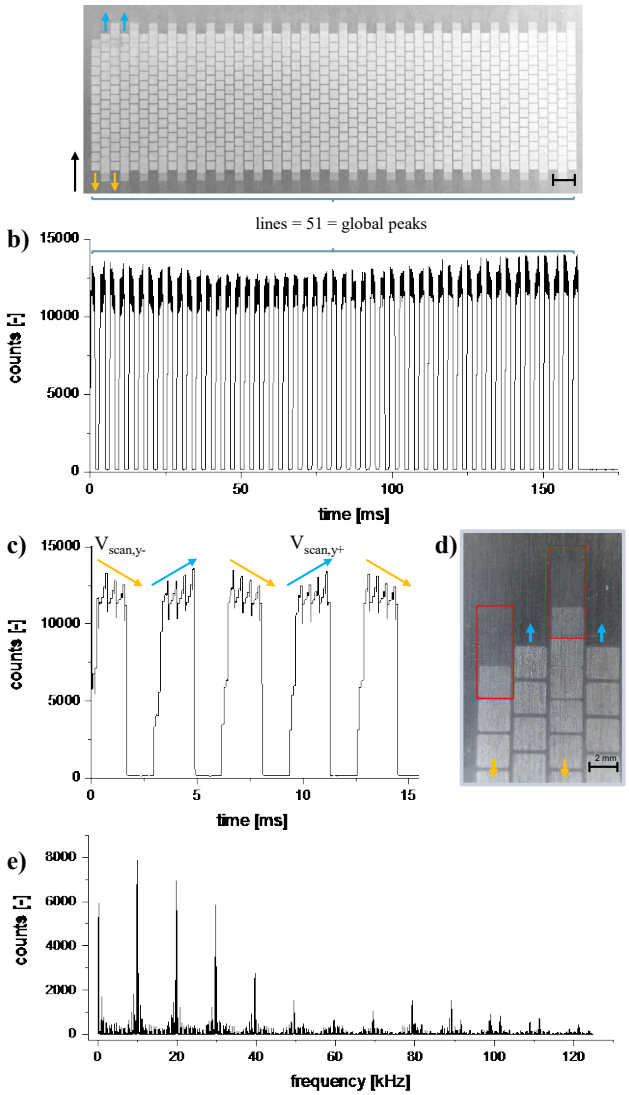

Fig. 5 (a) Photograph of a surface pre-treated with 983 W laser power and (b) corresponding signal response of electromagnetic emissions. (c) Magnified extract of signals for a detailed view, and (d) corresponding magnified macroscopic image. Arrows exemplary represent the scanning direction in y-direction. Red boxes exemplary mark the weak modified surface by the first three pulses in the corresponding line. (e) The absolute value of the FFT of the monitoring signal.

There are 51 global peaks in the signal, corresponding to the 51 pre-treated lines on the sample. Upon looking at the sensor's signal with higher resolution (see Fig. 5c), it is noticed that the global peaks consist of a rugged plateau. Within these rugged plateaus, a signal response was associated with each laser pulse striking the surface. Unexpectedly, the intensity of the signal corresponding to the first three pulses in each line rises until it reaches the plateau level. Also, the photograph of the treated surface (Fig. 5d) shows that the first three pulses did not modify the material as strong as the following pulses (see red markings in Fig. 5d). This finding can be explained by the turn-on characteristic of the laser source. Namely, every time the laser was turned on, it takes about three pulses until it reached a steady-state pulse energy. Considering the used scanning strategy, this behavior repeated in every new line. Therefore, the lower the energy that was provided by the laser to

modify the surface, the lower the resulting signal from the monitoring system.

Inspecting the signal in Fig. 5c, positive and negative slopes for each global peak can be also detected. The sign of the slope gives information about the scanning direction in y-direction, as a positive slope represents the laser beam moved in the positive y-axis, while a negative one implies a direction towards y = 0. This can be explained by the relative position of the radiation collecting units (see Fig. 1a) towards the y-axis origin. The closer the area under treatment to the position y = 0 was, the longer the distance between the processed spot and the collecting units was. Hence, the intensity of collected radiation, and thus the converted signal, was lower for pulses fired close to y = 0.

The fast Fourier transform (FFT, see Fig. 5e) of the signals provides information about the repetition rate of the laser during the pre-treatment process and the frequency of the completion of a single line. Considering exemplary signals obtained within Series 1, a dominant frequency of 10 kHz and the corresponding harmonics were noticed that can be correlated to the repetition rate of the laser. Also, a frequency of 312 Hz convoluted with the dominant frequency of 10 kHz and its harmonics were observed. This frequency of 312 Hz can be associated with the completion of a single line.

As discussed previously, employing different laser power has different impacts on the surface modification (see Fig. 2 - 4). The influence of three laser powers, namely 197 W, 590 W and 983 W, on the detected electromagnetic radiation can exemplarily be seen in Fig. 6a. The higher the laser power used, the higher the amplitude of the signals. In order to shed light on the dependence of the signal intensity as a function of the used power, additional experiments with 393 W and 786 W laser power were conducted. As shown in Fig. 6b, it was found that the average maximum intensities of the global peaks increased linearly with the used power ($R^2 = 0.95$).

In addition to varying laser power, geometrical irregularities on the surface can also have a significant impact on the resulting topography after the laser process and thus also on the emission of electromagnetic radiation during the treatment. Therefore, the laser pre-treatment of Al surfaces featuring geometrical irregularities represents another monitoring scenario which can be encountered in real environments.

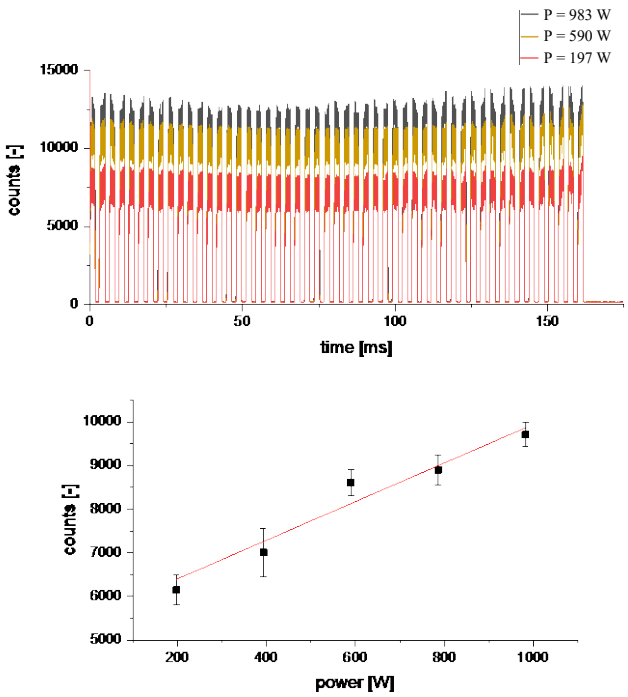

Fig. 6 (a) Signal of laser-based pre-treatment process using different laser power with a constant repetition rate f = 10 kHz with (b) the average intensities of the resulting signals including a linear fit ($R^2 = 0.95$).

Within the Series 2 of experiments, two flat overlapped aluminum sheets were tack welded (see Table 1, Series 2). An exemplary photograph of a resulting surface of Series 2 is shown in Fig. 7a, whereas the corresponding signal response of the detected electromagnetic radiations is presented in Fig. 7b. A region of interest in the macroscopic image and the corresponding region of the signal are marked with a red rectangle. A magnified view of this section is illustrated in Fig. 8a.

The fast Fourier transform (FFT, see Fig. 7c) of the signal shown in Fig. 7b can be analyzed analogously as for the experiments in Series 1. In this case, a dominant frequency of 20 kHz corresponding to the laser repetition rate, as well as their harmonics, can be detected. A frequency of 81 Hz associated to the completion of a single line can be detected as a convolution with the dominant frequency of 20 kHz and its harmonics.

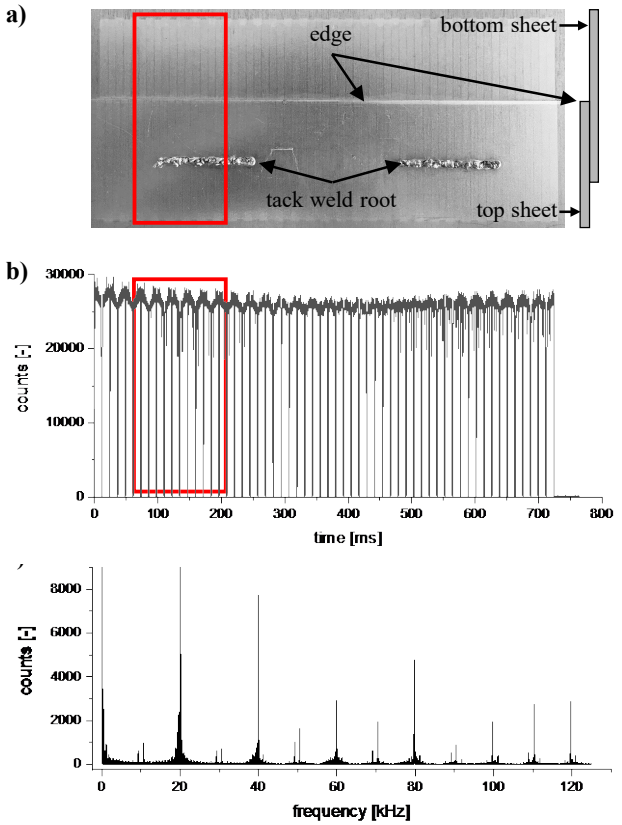

Fig. 7 (a) Macroscopic image including a schematical cross-section of overlapping sheets and (b) signal of samples processed with geometrical irregularities using a laser power of P = 1966 W, positive line/pulse overlap and a constant repetition rate f = 20 kHz. The signal section marked in red is illustrated in Fig.8a with higher magnification. (c) The absolute value of the FFT of the monitoring signal.

Using the laser parameters of Series 2 as described in Table 1, the courses of the detected signals are similar to those from Series 1 (see Fig. 5b). Due to the higher repetition rate in combination with a positive pulse overlap, each line was treated with approximately 200 more spots compared to Series 1 experiments. Therefore, in each global peak higher number of signal responses were observed. As a consequence of the higher applied laser power and positive overlap between pulses, the amplitude of the signals in general was significantly higher as in Series 1 (see Fig.7b).

As observed in the experiments of Series 1, the negative or positive slopes of the global peaks indicate the scanning direction used to process each line (see Fig. 8b). Detailed analysis of the signals indicates recurring sudden and steep drops and raises within their course but not within every global peak (see Fig. 8).

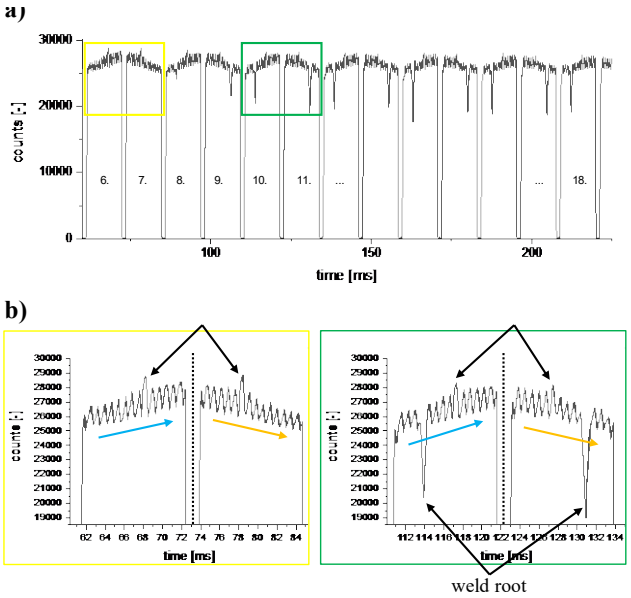

Fig. 8 (a) Detailed representation of exemplary signals detected while processing overlapping flat sheets with tack welds using P = 1966 W, f = 20 kHz, O_l = 15 %, and O_p = 90 %. (b) Global peaks featuring details on the irregularities of the surface. Arrows represent the scanning direction in ± y-direction.

These sudden drops and raises occur at positions where the laser irradiated the geometrical irregularities. The tack weld root caused the drop while the edge of the overlapping flat sheets of aluminum caused the raise within the corresponding global peak. A possible explanation for the drops can be the phenomenon described by Brown [45] and Bergström [46].

One portion of the radiation striking the rough and porous surface of the tack weld root can diffusively be reflected without reaching the detector. Another portion of the incoming light can be trapped in the cavities of the tack weld root, reflected multiple times within these cavities, and be guided into deeper layers of the material where it is absorbed. As the absorption takes place over a larger volume than on the flat surface and concurrently a faster heat dissipation might occur due to the larger effective area of the porous weld root, less IR heat radiation is emitted from the surface. Consequently, irradiation of the tack weld root resulted in a significant drop in the measured signal. In turn, when the laser beam interacted with the edge of the overlapping sheets, a significant portion of the radiation was reflected by the edge, causing the sudden increase in the intensity of the detected signal.

3.4 Online monitoring in industrial applications

In terms of online monitoring for industrial application, a process window needs to be set to establish the operational boundaries of the laser pre-treatment. It consists of several stages in accordance with the use case in a production line. An exemplary process window with four basic stages for the Series 2 of experiments is illustrated in Fig. 9. In this case the edge and the tack weld roots at the shown position (see Fig. 7 a) are known *a priori* and not considered to be undesired irregularities. The ideal process is accomplished once the signals stay within the first stage (see Fig. 9 a - 1). In case the signals exceed this first stage but

stay within the second stage (see Fig. 9 a - 2) a pre-warning appears. If the detected signals cross to the third stage (see Fig. 9 a - 3) the process will be aborted automatically. A "not ok" (nok) signal is reported, and an error is logged. Within the fourth stage (see Fig. 9 a – 4), the process is regularly expected to terminate, and the surface considered to be successfully processed. Hence, an "ok" signal is reported, and the successfully processed part will be sent to the next station in the production line for further processing such as adhesive bonding.

Each stage of the process window has to be developed by executing the process with the desired quality (including all desired features e.g. weld roots in correct position) in a high quantity. Furthermore, common scenarios with possible anomalies such as false tack weld positions and false laser power have to be reproduced within a high quantity of experiments, as well. The detected signals of these experiments are used as reference for a desired or undesired process. Hence, each stage of the process window is precisely matched to the reference signal received with a defined tolerance (see Fig. 9 b).

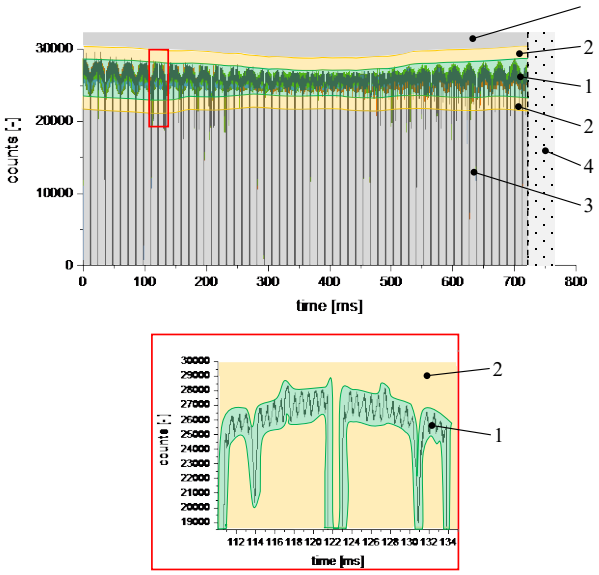

Fig. 9 (a) Exemplary process window of online monitoring in an industrial application with (b) magnified exemplary section – position marked in (a). Several stages of process windows are fitted as needed to the signal. With (1) desired area – signals within ideal process window, (2) pre-warning area – process tolerance window, (3), undesired area – signals below/above monitoring limit, and (4) regular process termination area – intended processing time reached. Each process window needs to be fitted accurately to the desired course of signals (b).

4. Conclusions

In this work, an innovative approach for temporal high-resolution online monitoring of an industrial laser-based pre-treatment process has been presented. The monitoring method has been evaluated in terms of the correlation of electromagnetic emissions and the quality of the resulting surfaces produced by a ns-pulsed laser beam ($\lambda = 1030$). The used monitoring system consisted of a photodiode-based sensor sensitive to electromagnetic radiation within a wavelength range between 750 nm and 1100 nm. The intensity of the resulting electrical signal correlated linearly with the used laser power whereas sudden drops and raises of the signal could be associated to the presence of geometrical irregularities. Moreover, the roughness parameters of the treated surfaces can be estimated from the signal intensity if a previous topographic characterization as function of laser power is performed. Analyzing the FFT spectrum of the recorded signals, it is also possible to monitor the relevant frequencies of the process, namely those associated to the laser repetition rate and the scanning of vertical lines. By filtering such frequencies, it is then possible to keep track of the stability of the process.

In conclusion, the approach based on the detection of electromagnetic radiations using diode-sensors is suitable for developing an online monitoring method such as a referential process window for industrial application.

Further research needs to be done using additional optical filters to analyze the electromagnetic radiations of different spectra separately. Spectroscopy measurements during the running process can help to distinguish which specific spectral ranges of electromagnetic radiations are emitted by the process.

Acknowledgments

The authors thank Uta Posselt, Julian Hackl, and Robert Schmid for their support in realizing numerous experiments.

References

[1] M. D. Banea, M. Rosioara, R. J. C. Carbas, and L. F. M. da Silva: Compos. Part B Eng., 151, (2018) 71.
[2] W. S. Miller, L. Zhuang, J. Bottema, A. J. Wittebrood, P. de Smet, A. Haszler, and A. Vieregge: Mater. Sci. Eng. A, 280, (2000) 37.
[3] B. Stojanović and B. Ivanović: Teh. Vjesn., 22, (2015) 247.
[4] H. Wan, J. Lin, and J. Min: Surf. Coat. Technol., 345, (2018) 13.
[5] H. Wan, J. Min, and J. Lin: Compos. Struct., 279, (2022) 114831.
[6] Y. Wu, J. Lin, B. E. Carlson, P. Lu, M. P. Balogh, N. P. Irish, and Y. Mei: Surf. Coat. Technol., 304, (2016) 340.
[7] G. Li, M. Lei, C. Liang, K. Li, B. Li, X. Wang, J. Wang, and Z. Wei: Appl. Sci., 12, (2022) 1199.
[8] R. Rechner, I. Jansen, and E. Beyer: Int. J. Adhes. Adhes., 30, (2010) 595.
[9] J. Min, H. Wan, B. E. Carlson, J. Lin, and C. Sun: Opt. Laser Technol., 128, (2020) 106188.
[10] R. Rechner, I. Jansen, and E. Beyer: J. Laser Appl., 24, (2012) 032002.
[11] M. Alfano, S. Pini, G. Chiodo, M. Barberio, A. Pirondi, F. Furgiuele, and R. Groppetti: J. Adhes., 90, (2014) 384.
[12] T. M. Yue, L. J. Yan, and C. P. Chan: Appl. Surf. Sci., 252, (2006) 5026.
[13] G. W. Critchlow, D. M. Brewis, D. C. Emmony, and C. A. Cottam: Int. J. Adhes. Adhes., 15, (1995) 233.
[14] M. Weck and C. Brecher: "Werkzeugmaschinen 3" ed. by M. Weck, (Springer Vieweg, Berlin, Heidelberg, 2006) p.267.
[15] T. Purtonen, A. Kalliosaari, and A. Salminen: Phys. Procedia, 56, (2014) 1218.
[16] L. Schmidt, F. Römer, D. Böttger, F. Leinenbach, B. Straß, B. Wolter, K. Schricker, M. Seibold, J. Pierre

Bergmann, and G. Del Galdo: Procedia CIRP, 94, (2020) 763.
[17] L. Zhang, A. C. Basantes-Defaz, D. Ozevin, and E. Indacochea: Int. J. Adv. Manuf. Technol., 101, (2019) 1623.
[18] R. J. Smith, M. Hirsch, R. Patel, W. Li, A. T. Clare, and S. D. Sharples: J. Mater. Process. Technol., 236, (2016) 93.
[19] M. Bastuck, H.-G. Herrmann, B. Wolter, P.-C. Zinn, and R.-K. Zaeh: Int. Congr. Appl. Lasers Electro-Opt., (2015) 410.
[20] N. Schroeder: J. Laser Micro Nanoengin., Ibaraki, 16 (2021) 130.
[21] S. Teutoburg-Weiss, B. Voisiat, M. Soldera, and A. F. Lasagni: Materials, 13, (2019) 53.
[22] G. Mallmann, R. Schmitt, and T. Pfeifer: ACTA IMEKO, 2, (2013) 73.
[23] G. Mallmann, R. Schmitt, K. Winands, and M. Pothen: Phys. Procedia, 39, (2012) 814.
[24] J. Endres, N. Kumar, P. Petrik, M.-. Henn, S. Heidenreich, S. F. Pereira, H. P. Urbach, and B. Bodermann: Proc. SPIE, Vol. 9132 (2014) 913208.
[25] F. Zechel, R. Kunze, P. Widmann, and R. H. Schmitt: Procedia CIRP, 94, (2020) 748.
[26] M. Zuric: J. Laser Micro Nanoengin., 14, (2019) 245.
[27] T. Steege, S. Alamri, A. F. Lasagni, and T. Kunze: Sci. Rep., 11, (2021) 14540.
[28] E. V. Bordatchev and S. K. Nikumb: Meas. Sci. Technol., 13, (2002) 836.
[29] Y. Cai and N. H. Cheung: Microchem. J., 97, (2011) 109.
[30] Y. F. Lu, M. H. Hong, S. J. Chua, B. S. Teo, and T. S. Low: J. Appl. Phys., 79, (1996) 2186.
[31] A. Papanikolaou, G. J. Tserevelakis, K. Melessanaki, C. Fotakis, G. Zacharakis, P. Pouli: Opto-Electron. Adv., 3, (2020) 19003701.
[32] S. Kradolfer, K. Heutschi, J. Koch, and D. Günther: Spectrochim. Acta Part B At. Spectrosc., 179, (2021) 106118.
[33] N. Schröder, G. Vergara, B. Voisat, and A. F. Lasagni: J. Laser Micro Nanoengin., 15, (2020) 150.
[34] J. H. Pak, S. Jeong, T. Lim, and S. Ju: Adv. Opt. Mater., 8, (2020) 1901706.
[35] D. V. Tran, Y. C. Lam, H. Y. Zheng, B. S. Wong, and D. E. Hardt: Appl. Surf. Sci., 253, (2007) 7290.
[36] D. Diego-Vallejo, D. Ashkenasi, and H. J. Eichler: Phys. Procedia, 41, (2013) 911.
[37] Md. H. A. Shaim and H. E. Elsayed-Ali: J. Appl. Phys., 122, (2017) 203301.
[38] R. Kunze, G. Mallmann, and R. Schmitt: Phys. Procedia, 83, (2016) 1329.
[39] DIN EN ISO 25178-6:2010-06, DOI: 10.31030/1555047.
[40] J. Meseguer, I. Pérez-Grande, and A. Sanz-Andrés: "Spacecraft Thermal Control", (Woodhead Publishing, Sawston, Cambridge, 2012), p.73.
[41] E. S. Gadelmawla, M. M. Koura, T. M. A. Maksoud, I. M. Elewa, and H. H. Soliman: J. Mater. Process. Technol., 123, (2002) 133.
[42] R. K. Leach: "Fundamental Principles of Engineering Nanometrology", (Elsevier, Amsterdam, 2010) p. 211.
[43] A. Naylor, S. C. Talwalkar, I. A. Trail, and T. J. Joyce: J. Funct. Biomater., 7, (2016): 9.
[44] E. Korin, N. Froumin, and S. Cohen: ACS Biomater. Sci. Eng., 3, (2017) 882.
[45] M. S. Brown and C. B. Arnold: "Laser Precision. Microfabrication" eds by K. Sugioka, M. Meunier, and A. Piqué, (Springer Vieweg, Berlin, Heidelberg, 2010), p.91.
[46] D. Bergström, J. Powell, and A. F. H. Kaplan: Appl. Surf. Sci., 253, (2007) 5017.

(Received: May 30, 2022, Accepted: October 31 , 2022)